Inorganic Chemistry

pubs.acs.org/IC Article

Tuning Magnetic Anisotropy in Co(II) Tetrahedral Carbazole-Modified Phosphine Oxide Single-Ion Magnets: Importance of Structural Distortion versus Heavy-Ion Effect

Gargi Bhatt, Tanu Sharma, Sandeep K. Gupta, Franc Meyer, Gopalan Rajaraman,* and Ramaswamy Murugavel*

Cite This: *Inorg. Chem.* 2023, 62, 18915−18925 Read Online

ACCESS | Metrics & More | Article Recommendations | Supporting Information

ABSTRACT: Three mononuclear cobalt(II) tetrahedral complexes $[Co(CzPh_2PO)_2X_2]$ ($CzPh_2PO$ = (9H-carbazol-9-yl)diphenylphosphine oxide and X = Cl (**1**), Br (**2**), I (**3**)) have been synthesized using a simple synthetic approach to examine their single-ion magnetic (SIM) behavior. A detailed study of the variation in the dynamic magnetic properties of the Co(II) ion in a tetrahedral ligand field has been carried out by the change of the halide ligand. The axial zero-field splitting parameter D was found to vary from −16.4 cm^{-1} in **1** to −13.8 cm^{-1} in **2** and +14.6 cm^{-1} in **3**. All the new complexes exhibit field-induced SIM behavior. The results obtained from ab initio CASSF calculations match well with the experimental data, revealing how halide ions induce a change in the D value as we move from Cl^- to I^-. The ab initio calculations further reveal that the change in the sign of D is due to the multideterminant characteristics of the ground state wave function of **1** and **2**, while single-determinant characteristics are instead observed for **3**. To gain a better understanding of the relationship between the structural distortion and the sign and magnitude of D values, magnetostructural D correlations were developed using angular relationships, revealing the importance of structural distortions over the heavy halide effect in controlling the sign of D values. This study broadens the scope of employing electronically and sterically modified phosphine oxide ligands in building new types of air-stable Co(II) SIMs.

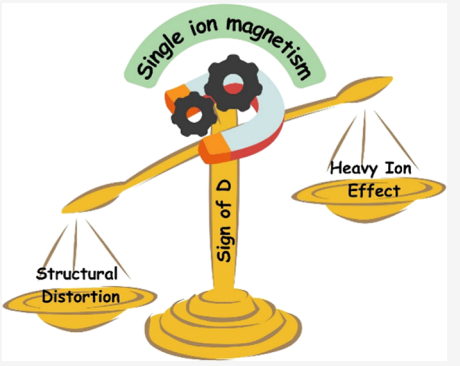

1. INTRODUCTION

The idea of persistent magnetism at the molecular level is changing the future of spintronics.[1] Designing molecules that exhibit insistent magnetic behavior has gained much attention during the past two decades. Such molecules, demonstrating magnetic bistability or slow relaxation of magnetization, are known as single-molecule magnets (SMMs).[2] The large negative axial zero-field splitting (ZFS) factor D is the key parameter for a material to exhibit SMM behavior.[3,4] In the past few years, there has been a shift in research toward mononuclear SMMs, which are referred to as single-ion magnets (SIMs). This shift is attributed to the fact that their magnetic properties can be altered through fine-tuning the design of the ligand field. Current efforts focus on identifying systems that possess substantial unquenched orbital angular momentum for increasing the barrier height of magnetization reversal (U_{eff}). On this ground, lanthanide-based SIMs are much superior owing to their significant first-order spin−orbit coupling (SOC) resulting in high magnetic anisotropy.[5,6] However, the realization of SMM properties for practical use becomes expensive in the case of lanthanide SIMs. On the other hand, transition metal (TM) ions are the best alternative for designing the cost-effective SIMs. They exhibit large crystal field splitting depending on the coordination environment of the central metal ion. The barrier height of TM SIMs depends on the second-order SOC. Thus, the ligand field and the coordination geometry play an important role in deciphering the anisotropy in TM SIM. In 2010, Long and co-workers[7] showed the presence of slow magnetic relaxation in mononuclear TM compound $[Fe^{II}(tpa^{Mes})]^-$, which led to the designing of several other 3d metal-based SIMs.[8] In recent years, the focus has however shifted to cobalt(II)[9−18] since it provides relatively large SOC and has inherent ground-state bistability from Kramer's degeneracy.[19−21] The record spin reversal magnetization (U_{eff}) value of 413 cm^{-1} for TM SIMs was reported by Gao et al. for the linear two-coordinate Co(II) complexes [(sIPrNHC)CoNDmp] (where sIPr = N-heterocyclic carbene and NDmp = arylimido ligand).[14] Subsequently, another linear Co(II) complex $[Co(C(SiMe_2Onaph)_3)_2]$ (where naph is a naphthyl group), which exhibits a spin

Received: July 13, 2023
Revised: October 14, 2023
Accepted: October 16, 2023
Published: November 10, 2023

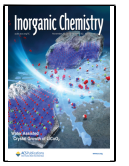

https://doi.org/10.1021/acs.inorgchem.3c02401
Inorg. Chem. 2023, 62, 18915−18925

reversal barrier of 450 cm^{-1}, was reported by Long and co-workers.[15] A recent synthesis of an air-stable Co(II) complex, $[L_2Co](TBA)_2$ (L = *N*,*N*′-chelating oxanilido ligand) by Meyer and co-workers, exhibiting slow relaxation dynamics (U_{eff} > 400 K and magnetic blocking up to 3.5 K) in the absence of an applied magnetic field, paves the path for the incorporation of a TM-based SIM on a surface.[18,22] It should be noted that, to date, desired high U_{eff} values have been achieved only in the case of unstable low-coordinate molecules at very low temperatures. Therefore, designing ambient stable SIMs that can be fabricated remains a challenge.[23,24]

Further, the geometry and coordination environment around the central metal ion play an important role in defining the SIM properties of the TM-based complexes.[25] Thus, the effects of the heavy donor atom,[11] halide ions,[26−31] and a secondary coordination sphere have been investigated to glean information for the rational design of newer SIMs. Fiedler and co-workers[32] recently studied the "heavy-atom effect" in high-spin cobalt(II)−halide complexes $[Co^{II}X(Tp^{tBu,Me})]$ ($Tp^{tBu,Me}$ is sterically hindered tris(pyrazolyl)-borato ligand), which have provided experimental basis to the fact that the choice of halide ions can modulate ZFS owing to the ligand field effects.

Cobalt(II), being an intermediate acid, can bind to a variety of donor atoms, and the effect of halide ions on the electronic structure of cobalt ions has been studied widely with phosphine-based complexes and various other ligands.[19] A nonexhaustive list of tetrahedral complexes of Co(II) having halide ion ligation in primary coordination and $\{CoL_2X_2\}$ cores with L being donor atoms and X being halogen atoms is given in Table 1. Despite the vast interest in both tetrahedral Co(II) and phosphine oxide ligands, there are no examples of magnetic studies of structurally characterized complexes combining cobalt(II) and phosphonamide or even simpler phosphine oxide ligands in tetrahedral geometry (Chart 1).[33] In this regard, three mononuclear tetrahedral cobalt(II) complexes $[Co(L)_2X_2]$, where L= (9*H*-carbazol-9-yl)-diphenylphosphine oxide and X = Cl, Br, I] have been synthesized in the present study to acquire information about their SIM behavior.

Table 1. Nonexhaustive List of Tetrahedral Co(II) Complexes with Halide Ion Substitution in the Primary Coordination Sphere for the $\{CoL_2X_2\}$ Core

complex	*D* value (cm^{-1})	U_{eff} (K)	τ_0 (s)	Reference
$[CoL'X_2]$ (L′ = 9,9-dimethyl-4,5-bis(diphenylphosphino)xanthene)				
X = Cl	−15.1	25.5	2.7×10^{-6}	35
X = Br	−11.6	18.7	1.8×10^{-6}	35
X = I	−7.3	9.2	1.2×10^{-6}	35
$[CoX_2(H_2thp)_2]$ (H2thp = 2-(1,4,5,6-tetrahydropyrimidin-2-yl)phenol)				
X = Cl	−12.9	27.769	4.74×10^{-10}	36
X = Br	−20.9	53.09	1.00×10^{-9}	36
X = I	−19.0			36
CoX_2 $^{Dipp}MIC_2$ (MIC = mesoionic carbene)				
X = Cl	−6.54			37
X = Br	−8.27			37
X = I	−9.67			37
$[CoX_2(qu)_2]$ (qu = quinoline)				
X = Cl	−5.16			38
X = I	+9.2			11
$[CoX_2(PPh_3)_2]$				
X = Cl	−11.6	37.1	1.2×10^{-9}	39,40
X = Br	−12.5	37.3	9.4×10^{-11}	27
X = I	−36.9	30.6	4.65×10^{-10}	11
$[Co(biq)X_2]$ (biq = 2,2′-biquinoline)				
X = Cl	+10.5	42.6	1.9×10^{-10}	41
X = Br	+12.5	39.6	1.2×10^{-10}	41
X = I	+10.3	57	3.2×10^{-13}	41
$[Co(L'')_2X_2]$ (L″ = tetramethylthiourea ($[(CH_3)_2N]_2C$ = S))				
X = Cl	−18.1	37.69	3.69×10^{-10}	28
X = Br	−16.4	32.94	2×10^{-8}	28
X = I	−22	39.99	1.22×10^{-6}	28
$[Co(L''')_2X_2]$ (L‴ = thiourea $[(NH_2)_2C$ = S {10% dilute sample})				
X = Cl	+17.4	39.13	2.29×10^{-10}	28
X = Br	±14.9	38.991	3.3×10^{-9}	28
X = I	−18.3	47.048	2.29×10^{-10}	28
$[Co(CzPh_2P(O))_2X_2]$				
X = Cl (**1**)	−16.4	30.9	1.11×10^{-9}	this work
X = Br (**2**)	−13.8	21.7	8.36×10^{-9}	this work
X = I (**3**)	+14.6	35.1	4.15×10^{-10}	this work

2. RESULTS

2.1. Synthesis. The phosphoryl P═O group coordinates strongly with the divalent TM ions that are neither too hard nor too soft. The bulky phosphine oxide ligands are used to avoid the adoption of larger coordination numbers (for instance, five or six coordination numbers in the case of 3d metal ions). Furthermore, the introduction of bulky groups on phosphorus increases the distance between the two metal centers in the lattice and hence decreases the intermolecular interactions. Accordingly, the bulky (9*H*-carbazol-9-yl)-diphenylphosphine oxide (L) was prepared by an earlier reported method.[34] The reaction of anhydrous CoX_2 (X = Cl, Br, and I) with L in dry toluene under a nitrogen atmosphere results in the formation of tetrahedral cobalt(II) complexes as crystalline products (Scheme 1). Compounds **1**−**3** have been characterized by spectroscopic and analytical methods. Their molecular structures have been confirmed by single-crystal X-ray diffraction studies.

2.2. Crystal Structures of 1−3. Single-crystal X-ray diffraction studies reveal that complexes **1** and **2** crystallize in the triclinic space group $P\bar{1}$, while complex **3** crystallizes in the monoclinic *C*2/*c* space group, although all three complexes are isostructural. The Co(II) center is coordinated by two oxygen atoms of the ligand (L) and two terminal ligands X (X = Cl^- (**1**), Br^- (**2**), and I^-(**3**)) (Figure 1). The local symmetry of the cores $\{CoO_2X_2\}$ is pseudotetrahedral (T_d). The cobalt ion interacts stronger with the phosphoryl oxygen of the ligand with bond lengths of 1.959(2) and 1.983(2) Å for **1**, 1.955(5) and 1.972(5) Å for **2**, and 1.978(2) Å for **3**; the bond lengths to the X ions are 2.2175(9) and 2.2189(4) Å for **1**, 2.355(1) and 2.364(2) Å for **2**, and 2.582(4) Å for **3**. The Co−X bond distances increase as the ionic radius of the terminal atom (X) increases (Table S3). The X−Co−X angles are 120.85(4)° for **1**, 120.46(5)° for **2**, and 111.77(3)° for **3**. There is considerable widening of the X-Co-X angle from the ideal tetrahedral angle for **1** and **2** (X = Cl and Br) compared to that for **3**.

Mononuclear units in the structures of **1**−**3** are well isolated from each other, with the shortest Co···Co separations being greater than 9 Å. Thus, the shortest intermolecular Co−Co distances observed are 9.7909(7), 9.8107(15), and 9.7090(3) Å for **1**, **2**, and **3**, respectively. There are no intermolecular or intramolecular hydrogen bonding or arene−arene π interactions present in any of the three complexes.[42] A comparison

https://doi.org/10.1021/acs.inorgchem.3c02401
Inorg. Chem. 2023, 62, 18915−18925

Chart 1. Representative examples of tetrahedral Co(II) phosphine and phosphine oxide complexes $[CoL_2X_2]$ (types i–iii) investigated for their SIM behavior. Surprisingly, simple Co(II) tetrahedral systems that contain monodentate phosphine oxides $R_3P = O$ as ligands (type iv) in the above scheme have not been investigated for their magnetic behavior.

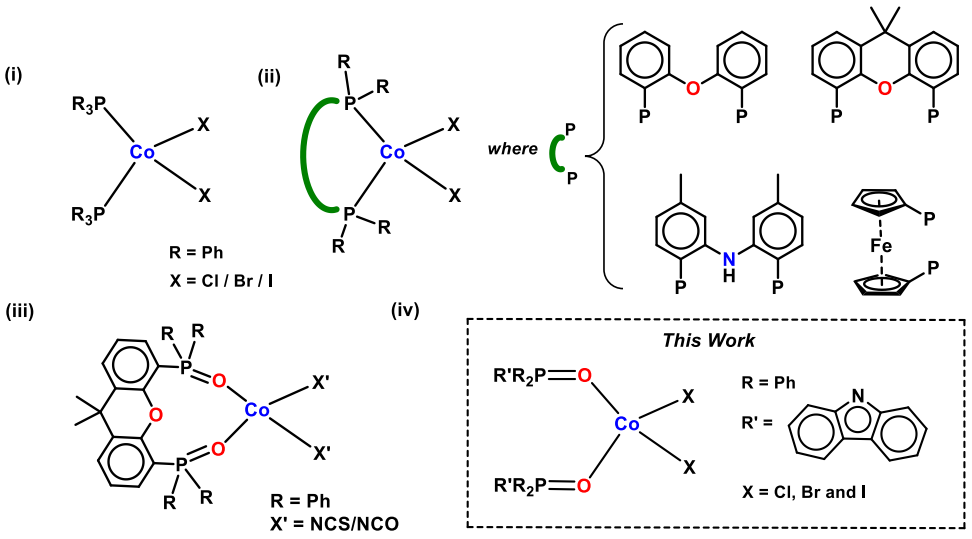

Scheme 1. Synthesis of Complexes 1–3

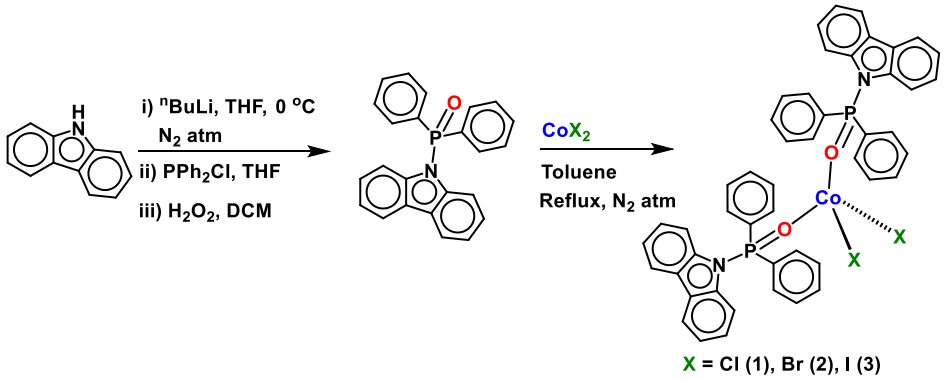

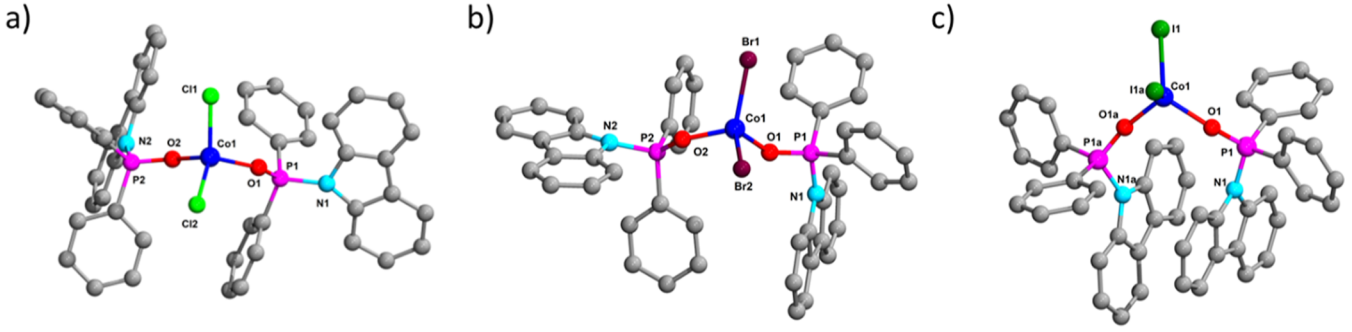

Figure 1. Molecular structures of (a) **1**, (b) **2**, and (c) **3** (the hydrogen atoms have been omitted for the sake of clarity).

among the complexes can be made based on their significant structural parameters shown in Table S3. In order to provide more insights into the coordination geometries, continuous shape measurement has been performed,[43] which shows that all Co (II) centers have distorted tetrahedral geometries (Figure 2) with minimum deviation factors of 0.996, 1.512, and 2.156 for **1**, **2**, and **3**, respectively. The detailed analyses are given in Table S4.

2.3. Static Magnetic Properties. The magnetic studies on complexes **1–3** were performed on polycrystalline powdered samples. At 200 K, the $\chi_M T$ value of 2.73 cm^3 K mol^{-1} for **1** (Figure 3) is higher than the expected spin-only value (1.875 cm^3 K mol^{-1}) for one isolated and noninteracting high-spin Co(II) ion ($S = 3/2$, $g = 2.0$) indicating significant orbital contribution to the magnetic moment, resulting from the ligand-field-induced structural distortion of the tetrahedral symmetry. The $\chi_M T$ value remains almost constant until 50 K before sharply decreasing to 1.55 cm^3 K mol^{-1} at 2 K. The sharp decline in the $\chi_M T$ value below 50 K can be due to the presence of ZFS. The intermolecular interactions can be considered very weak as the intermetallic distance between the Co(II) ions in the lattice is 9.791 Å. The magnetization for **1**

https://doi.org/10.1021/acs.inorgchem.3c02401
Inorg. Chem. 2023, 62, 18915–18925

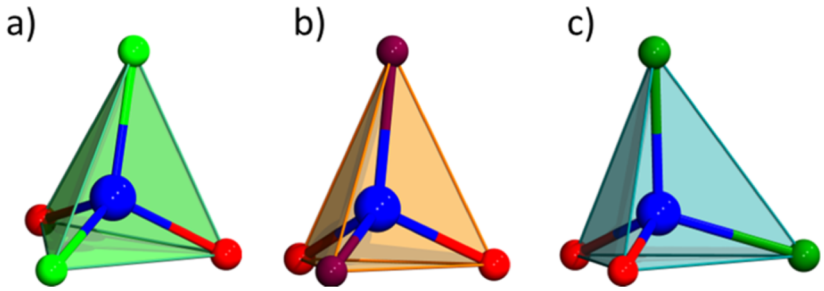

Figure 2. Distorted tetrahedral coordination around Co(II) centers in (a) **1**, (b) **2**, and (c) **3**.

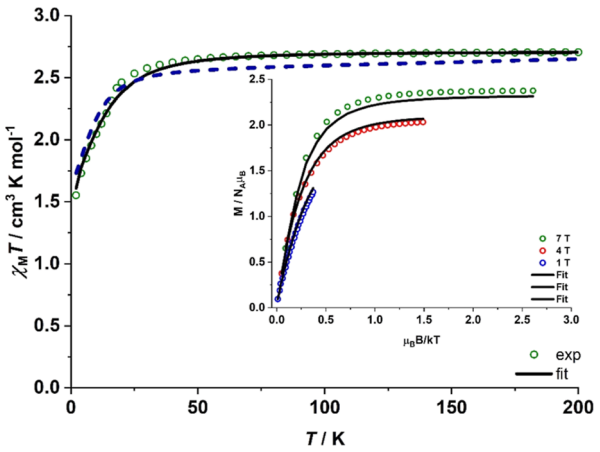

Figure 3. Variable-temperature $\chi_M T$ product for **1** measured under an applied dc field of 0.5 T. The solid line is the best fit, and the dashed line is the theoretical prediction with CASSCF/NEVPT2. Inset: Variable-temperature variable-field magnetization for complex **1**. The solid lines are the best fits.

increases linearly up to 1.5 T and then gradually reaches 2.35 μ_B at 7 T without complete saturation (Figure S7), much below the expected value of 3.0 μ_B for an isolated Co(II) ion (S = 3/2, g = 2.0) system. The magnetic susceptibility data were fitted along with the variable-field variable-temperature magnetization data (Figure 3 inset) with julX_2s[44] using the spin Hamiltonian in eq 1

$$\hat{H} = D\left[\hat{S}_z^2 - \frac{1}{3}S(S+1)\right] + E(\hat{S}_x^2 - \hat{S}_y^2) + \mu_B \vec{B}\mathbf{g}\hat{\mathbf{S}} \quad (1)$$

where D and E represent the axial and the rhombic ZFS parameters. S, S_x, S_y, and S_z represent the total spin and its x, y, and z components, respectively. μ_B, g, and B represent Bohr's magneton, the Zeeman anisotropic interaction tensor, and the magnetic field vector. The best fit yields D = −16.4 cm^{-1}, E/D = 0.07, and g = 2.40 (Figure 4).

The χ_MT value also remains almost constant for complexes **2** (Figure S8) and **3** (Figure S11) until 50 K before a gradual decrease at lower temperatures. The χ_MT values for complexes **2** and **3** are 2.67 and 2.69 cm^3 K mol^{-1} at 200 K and 1.58 and 1.65 cm^3 K mol^{-1} at 2 K, respectively. The simultaneous fitting of the magnetic susceptibility and variable-temperature variable-field magnetization data (Figure S9 for **2** and S12 for **3**) yields D = −13.8 cm^{-1}, E/D = 0.14, and g = 2.39 for **2** and D = +14.6 cm^{-1}, E/D = 0.26, and g = 2.41 for **3**, respectively. It is interesting to note that the sign for the ZFS parameter D changes from negative to positive while changing the coordinating halide from lighter chloride to heavier iodide. This is contrary to that observed for other reported halide tetrahedral complexes.[11,35,37−39] The ab initio calculations carried out using the CASSCF/NEVPT2 method on the crystallographic coordinates (see next section for details) agree well with the experimental results. Table 2 summarizes the magnetic parameters determined by SQUID magnetometry and theoretical calculations. Figures S20−S22 show the error surface and dependence of the extracted parameters, suggesting the sensitivity of the sign of D with respect to the static magnetic data. These parameters are consistent with those reported for other tetrahedral cobalt(II) complexes.

2.4. Dynamic Magnetic Properties. To further understand the effect of the coordinating halide ions on the dynamics of slow relaxation of magnetization, ac susceptibility measurements were performed on the polycrystalline samples in the frequency range of 0.1−1000 Hz (Figure 4). Complexes **1**−**3** did not exhibit any slow relaxation in the absence of an external applied magnetic field in the operating temperature range of our SQUID magnetometer (Figure S14). This is on expected lines based on the large rhombicity observed in all the complexes (E/D = 0.056−0.261, see Table 2), leading to the mixing of the spin states and the hyperfine interactions typically present in Co(II) complexes. Application of an optimum dc field (Figure S15) of 1000 Oe substantially quenches the fast relaxation processes in complex **1**, and thus, maxima were observed in the frequency-dependent out-of-phase (χ_M'') component of ac susceptibilities up to 2.5 K (Figure 4a). The semicircular χ_M'' versus χ_M' curves (Figure 4c) were fitted with the generalized Debye function, and the relaxation rates (τ) were extracted.[45] The α parameter lies in a narrow range 0.027−0.147. The relaxation rates (τ^{-1}) were analyzed with the following function

$$\frac{1}{\tau} = \frac{1}{\tau_{QTM}} + AH^4T + CT^n + \frac{1}{\tau_0}\exp\left(\frac{-U_{eff}}{k_BT}\right) \quad (2)$$

where the four terms represent magnetic relaxation through QTM, direct, Raman, and Orbach mechanisms, respectively. Fitting the temperature dependence of relaxation rates using only direct and Raman mechanisms along with QTM was unsuccessful. τ^{-1} versus T obtained under the applied dc field could however be reproduced well using a combination of direct and Orbach relaxation mechanisms. The best fit yields A = 241,389 K^{-1} T^{-4} s^{-1} and U_{eff} = 28.9 K with $\tau_0 = 2.51 \times 10^{-9}$ s (Figure 5d).

Similarly, the application of an optimum external magnetic field of 1000 and 800 Oe in the case of complexes **2** (Figure S16) and **3** (Figure S18) leads to the observance of frequency-dependent maxima in the χ_M'' component of the ac susceptibilities up to 2.1 and 2.7 K, respectively (Figures S17 and S19). The α parameter lies in a narrow range of 0.08−0.03 and 0.057−0.026 for **2** and **3**, indicating a narrow distribution

https://doi.org/10.1021/acs.inorgchem.3c02401
Inorg. Chem. 2023, 62, 18915−18925

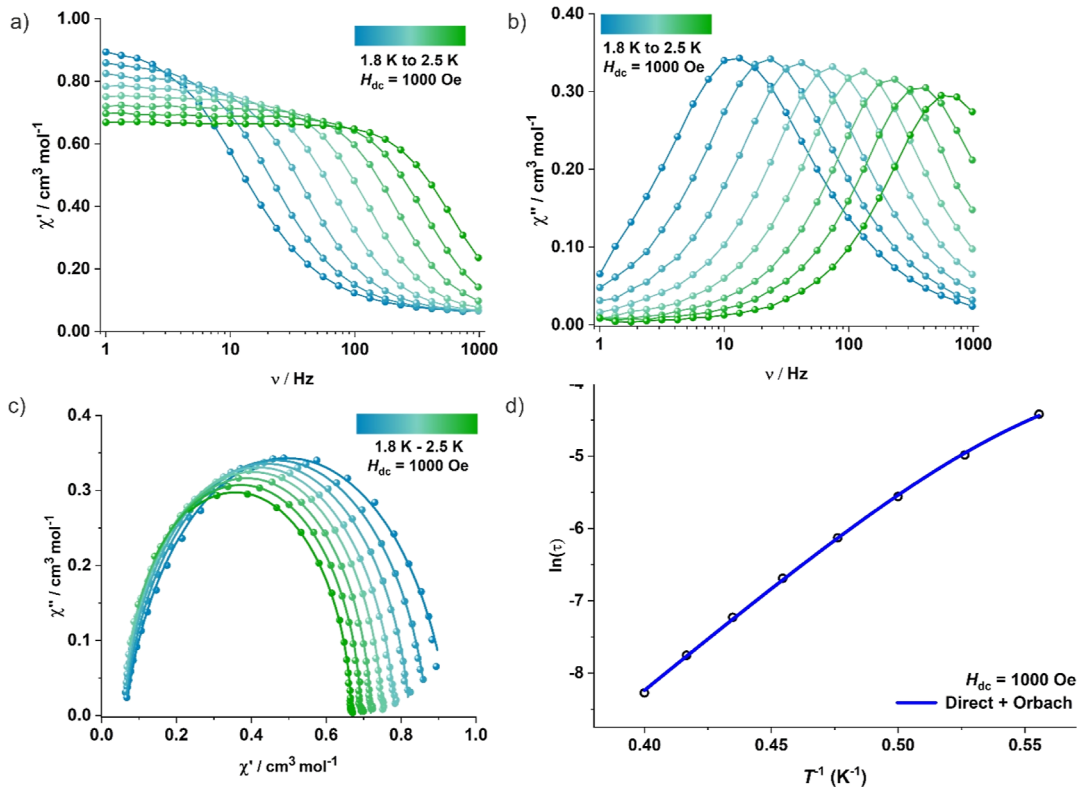

Figure 4. (a) In-phase (χ_M') and (b) out-of-phase (χ_M'') components of the frequency-dependent (0.1−1000 Hz) ac susceptibility measured in an oscillating ac field of 3.0 Oe and an applied dc field of 1000 Oe for **1**. (c) Cole−Cole plots for **1** under an applied dc field of 1000 Oe. (d) Plot of the relaxation time τ (logarithmic scale) versus T^{-1} for **1**. The solid blue line represents the best fitting to the direct and Orbach mechanism.

Table 2. Summary of the Various Magnetic Parameters Determined Experimentally and Obtained by CASSCF/NEVPT2

							CASSCF/NEVPT2	
comp	g	D (cm^{-1})	E/D	U_{eff} (K)	τ_0 (s)	H_{dc} (Oe)	D (cm^{-1})	E/D
1	2.40	−16.4	0.07	28.9	2.51×10^{-9}	1000	−10.5	0.25
2	2.39	−13.8	0.14	22.7	5.19×10^{-9}	1000	−5.2	0.27
3	2.41	+14.6	0.26	30.9	2.05×10^{-9}	800	+12.2	0.15

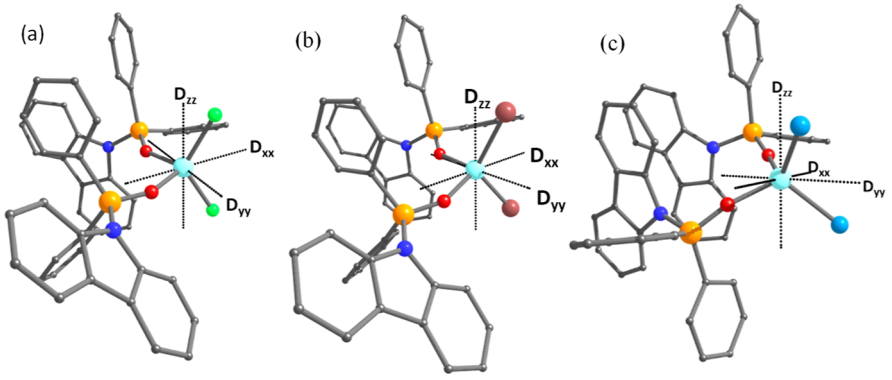

Figure 5. NEVPT2-calculated orientation of the main magnetic axes (D tensor) for (a) **1**, (b) **2**, and (c) **3**. Color code Co (cyan); O (red); Cl (green); Br (brown); I (sapphire blue); N (blue); C (gray); and P (orange). Here, hydrogens are omitted for clarity.

of relaxation time. The best fit yields A = 366,080 K^{-1} T^{-4} s^{-1}, U_{eff} = 22.7 K with $\tau_0 = 5.19 \times 10^{-9}$ s for **2** and A = 588,620 K^{-1} T^{-4} s^{-1}, U_{eff} = 30.9 K with $\tau_0 = 2.05 \times 10^{-9}$ s for **3**.

Furthermore, to confirm the sign of D, Q-band EPR studies were carried out for **2** and **3** with one exhibiting negative D and the other positive D with a pseudo-S = 1/2 stabilized in the case of the latter (however, **1** did not give reasonable EPR spectra at 5 K). The pseudo S = 1/2 ground state is expected to yield a signal around $g \sim 2.00$ in tetrahedral Co(II) complexes. The EPR spectrum of **3** resembles the earlier reports of Co(II) complexes with the positive D value[46,50] (Figure S24). This measurement provides compelling evidence of a $g \sim 2.2$ signal for complex **3**, whereas this signal is noticeably absent in the case of complex **2**. This finding

https://doi.org/10.1021/acs.inorgchem.3c02401
Inorg. Chem. 2023, 62, 18915−18925

corroborates the anticipated sign of ZFS as predicted by the theoretical calculations.[28,50]

2.5. Estimation of ZFS Parameter Using Ab Initio Calculations. Ab initio calculations based on CASSCF/NEVPT2 utilizing ORCA suite of programs were performed to estimate the D, E/D, and g values in complexes **1** through **3** (see Table 2). The computed values match with the experimental susceptibility data (see Figures 3, S7, S10, and Table 2) Figure 4). For a complex having ideal T_d symmetry, the ligand field terms are $^4A_2(F)$, $^4T_2(F)$, and $^4T_1(P)$; however, as complexes **1**−**3** are having only a pseudo C_2 symmetry, the terms transform into ^4A, [^4A and two ^4B](F), and [^4A and two ^4B](P) states, respectively. The three states [^4A and two ^4B terms](F) that arise from the $^4T_2(F)$ term become the first excited states, whereas the ^4A term resulting from $^4A_2(F)$ term becomes the ground state.

Figure 5 depicts the orientation of D for complexes **1**−**3**. The E/D value was found to increase from complex **1** to complex **3**. Due to variations in the excitation from the d_{xz} and d_{yz} orbitals of the t_2 subshell (Figures 6 and 7), the D_{XX} and

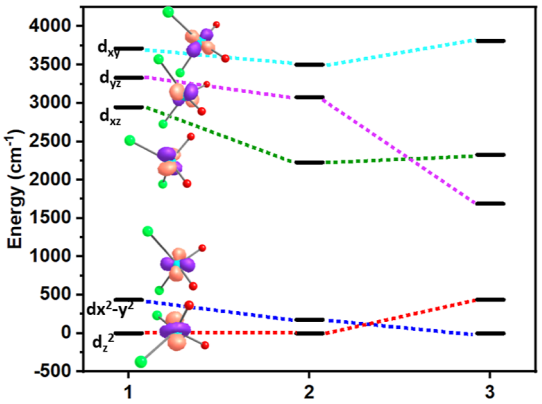

Figure 6. Comparative energies of the d orbitals in complexes **1**−**3**; only the core structures are shown. Color code Co (cyan); O (red); and X (green). Contour plots of the d orbitals (isosurface 0.1 e^- $bohr^{-3}$) corresponding to the energy levels are shown along.

D_{YY} components differ. The considerable splitting between the d_{xz} and d_{yz} orbitals leads to a large contributional difference to the D_{XX} and D_{YY} components, which accounts for the high $|E/D|$ values. The presence of two different donor atoms with distinct σ/π-donor properties leads to a significant splitting between the d_{xz} and d_{yz} orbitals in **1** to **3** (Figure 6). All these complexes exhibit a significant splitting between these two orbitals due to interactions between the d_{xz} orbital and an oxygen atom and the d_{yz} orbital and an X^- ion.

The state-wise contributions to the D values arising from various excitations are shown in Table 3. It is well-known that the transition between orbitals with two distinct m_l values contributes to the positive D value, and the spin-conserved transition between orbitals with the same m_l value contributes to the negative D value.[25,28,47−50] It is clear from the data presented in Table 3 that the major contribution to D originates from the $^4T_2(F)$ state. For **1** and **2**, first two major contributions from the $^4T_2(F)$ state are negative but positive for **3**. On going from **1** to **3**, there is reduction in the negative contribution to the D value. For **1** and **2**, the ground-state wave function exhibits strong multideterminant characteristics. The electronic configuration of the ground state of **1** is $[(d_z^2)^1(dx^2\text{-}y^2)^2((d_{xz})^1(d_{yz})^2(d_{xy})^1]$ (33%), whereas the first excited state is $[(d_z^2)^1(d_{x^2-y^2})^1((d_{xz})^1(d_{yz})^2(d_{xy})^2]$ (51%). Similarly, for **2**, the ground state and first excited state are $[(d_z^2)^1(d_{x^2-y^2})^2((d_{xz})^1(d_{yz})^2(d_{xy})^1]$ (32%) and $[(d_z^2)^1(d_{x^2-y^2})^1((d_{xz})^1(d_{yz})^2(d_{xy})^2]$ (39%), respectively (Figure 7). This suggests that complexes **1** and **2** have a strong multideterminant character at the ground and excited states. In contrary, the ground state of **3** portrays the single-determinant characteristics.

In complexes **1** and **2**, large contributions to D were found to arise from the same m_l value orbitals, i.e., $d_{x^2-y^2} \rightarrow d_{xy}$ (Figure 7), but in **3**, the majority of the contributions arise from the transition between different m_l levels. Generally, heavier halide offers weaker ligand field stabilizing excited states closer to the ground state, enhancing their contributions, and hence typically, they exhibit a negative D value. However, in this set of complexes studied, this is not the case. To understand the origin of variation in the sign of D, beyond the variations in the transition between the same m_l versus different m_l orbitals, we explored the role of structural distortions brought in due to the presence of halide ions. Two sets of models were studied, first the role of the O donor in stabilizing negative versus positive D values. To investigate this effect, the O donors in complexes **1**−**3** were replaced by S atoms generating models $\mathbf{1}_S$, $\mathbf{2}_S$, and $\mathbf{3}_S$. Second, the X-Co-X angles in complexes **1**−**3** are drastically different. To study the role of this angle and isolate the role of heavier halide ions in dictating the D value, we have replaced the Cl^- ion in complex **1** by the I^- ion keeping the Co−I distance the same as that of complex **3** (model $\mathbf{1}_I$) and vice versa (model $\mathbf{3}_{Cl}$). Further magnetostructural correlations for the X−Co−X angles were developed on complex **3** to further understand the role of this angle in dictating the D and $|E/D|$ values.

Table 4 reveals that models $\mathbf{1}_S$, $\mathbf{2}_S$, and $\mathbf{3}_S$ exhibit the negative D values. As can be predicted, these values are higher than those of structures **1**−**3** due to the heavy-ion effect, but the trend is still consistent with that of **1**−**3**., i.e., $\mathbf{3}_S$ is less negative than $\mathbf{1}_S$, suggesting that the softer ligand such as S^{2-} in combination with I^- does not necessarily yield larger negative D as one assumes, indicating that the geometry plays a critical role in dictating both the magnitude and the sign. The estimated D values for $\mathbf{1}_I$ and **1**, respectively, are −8.58 cm^{-1} and −12.62 cm^{-1}, and 4.1 cm^{-1} observed between the two shows the impact of heavy ions in action. Similarly, between $\mathbf{3}_{Cl}$ and **3**, the difference D is estimated to be ∼3.0 cm^{-1}. This suggests that heavier ions tend to increase the negative contribution to D by ∼3−4 cm^{-1}, and if the difference in the D value among various halide compounds is smaller, this can result in a switch in the sign of D as observed in earlier reports.[46,51] The X-Co-X angle however plays a crucial role in dictating the D value. To further understand the role of this angle, magnetostructural correlations were developed.

2.6. Magnetostructural D Correlation. Magnetostructural correlation has been performed on **3** to comprehend how structural factors affect the sign and amplitude of the D value in tetrahedral Co^{II} complexes. To create tetragonally compressed and elongated structures, we systematically altered the O−Co−O and X−Co−X bond angles. These alterations are made along the C_2 axis, which also coincides with the D_{zz} axis shown in Figure 5. The distortion in the tetrahedral structure is defined as $\delta = 2 \times 109.5° - (\alpha+\beta)$ (where α = O−Co−O angle and β = X−Co−X). Tetrahedral geometry is flattened when δ is negative, whereas tetragonally elongated geometry is represented by a positive δ value. The δ values varied from

https://doi.org/10.1021/acs.inorgchem.3c02401
Inorg. Chem. 2023, 62, 18915−18925

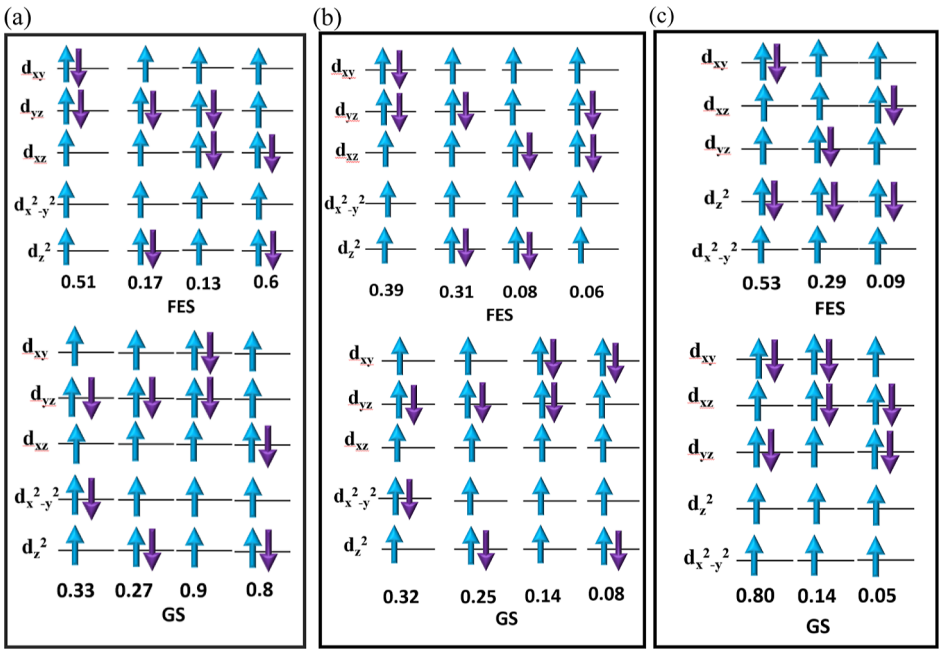

Figure 7. Ground-state (GS) and first excited-state (FES) configurations computed for complexes (a) **1**, (b) **2**, and (c) **3**.

Table 3. State-by-State Contributions to the *D* Values [cm^{-1}] and the SH Parameters (g, D, $|E/D|$) Were Estimated via CASSCF (7, 5)+NEVPT2

	1		2		3	
state	CASSCF	NEVPT2	CASSCF	NEVPT2	CASSCF	NEVPT2
$^4T_2(F)$	−29.03	−23.11	−8.08	−13.88	28.01	19.23
	18.49	14.75	9.74	8.60	24.35	18.49
	−4.22	−3.6	−5.44	−5.29	−22.43	−16.65
	1.24	1.38	−3.39	4.98	−13.39	−8.89
^2G	4.06	4.14	2.09	3.09	4.58	4.64
	−2.89	−2.95	−2.19	−2.15	−2.34	−2.41
D_{tot}	−12.62	−10.54	−6.15	−5.15	16.67	12.20
$\|E/D\|$	0.21	0.26	0.28	0.27	0.29	0.15
g_{xx}	2.325	2.261	2.384	2.301	2.616	2.441
g_{yy}	2.385	2.316	2.418	2.329	2.339	2.264
g_{zz}	2.497	2.402	2.465	2.366	2.488	2.389

Table 4. CASSCF- and NEVPT2-Computed SH Parameters (D and $|E/D|$)

complex	D $(cm^{-1})_{casscf}$	$\|E/D\|_{casscf}$	D $(cm^{-1})_{NEVPT2}$	$\|E/D\|_{NEVPT2}$
1	−12.62	0.21	−10.5	0.25
2	−6.15	0.28	−5.1	0.27
3	16.67	0.29	12.2	0.15
$\mathbf{1}_S$	−38.81	0.15	−27.5	0.20
$\mathbf{2}_S$	−35.90	0.13	−24.3	0.21
$\mathbf{3}_S$	−20.40	0.28	−16.5	0.21
$\mathbf{1}_I$	−8.58	0.08	−3.8	0.14
$\mathbf{3}_{Cl}$	13.58	0.27	11.4	0.23

−50° to +50° in complex **3**. It was observed that with the negative δ values, we observe the negative D values, whereas for the δ values in the range of 10−20°, the D turns positive (Figure 8). The D again turns negative for the δ value in the range of +30−50°. The D value is the largest when the δ value is −50.

The total axiality of the estimated D value drops as we move from flattened to perfect tetrahedral shape (increasing value)

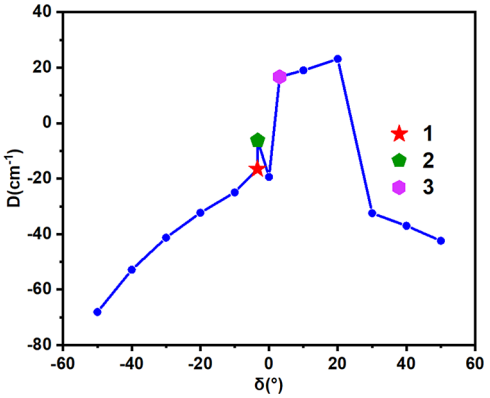

Figure 8. Variation of the D values with changing δ value along with the corresponding parameters observed for **3**. The D value observed is mapped (closed blue circles). The red star shows the D value of **1**, green pentagon **2**, and magenta hexagon **3**.

(Figure 8). When the geometry is ideal tetrahedral, the sign of D changes from negative to positive. A positive D value is

https://doi.org/10.1021/acs.inorgchem.3c02401
Inorg. Chem. 2023, 62, 18915−18925

observed for the δ values of 0 to +20. The easy-axis anisotropy is stabilized once more by a further increase in the value beyond +30. Notably, the magnetostructural correlation investigated here maintains consistency with similar molecules,[28,46] although it diverges when considering molecules utilizing different ligand systems.[52] The δ values of complexes **1**−**3** are estimated to be −3.4, −3.3, and 3.1°, respectively. If 3−4 cm^{-1} of the heavier ion effects are subsumed, the δ value can easily explain the variation in the sign of D as we move from Cl^- to I^-, suggesting that the structural distortion that is brought in by the halide ion is key to the estimation of D rather than the secondary spin−orbit effects offered by these ions.

3. DISCUSSION

The effects of donor-atom size and coordination number on the electronic, magnetic, and structural properties of high-spin cobalt(II)−halide complexes supported by substituted phosphine oxide ligands have been investigated in the present work. The study involved a series of four-coordinated complexes, which were characterized with X-ray crystallography. Complexes **1**−**3** possess two significant features compared to Co(II)-SIMs earlier reported with the CoL_2X_2 core. First, the ligands in complexes **1**−**3** contain phosphoryl oxygen atoms as two of the donor sites, which is an uncommon feature among four-coordinate Co(II)-SIMs. Most of the four-coordinate Co(II)-SIMs reported in the literature have ligands that coordinate with N, P, As, S, Se, and/or halide atoms as donor sites (Table 1). The presence of phosphoryl oxygen atoms in the ligands of complexes **1**−**3** affects the electronic and steric environment around the central cobalt ion, which significantly impacts the magnetic and structural properties of these complexes. Second, the hard nature of oxygen provides a strong and stable bond with the metal ion, which can lead to increased thermal stability and a longer lifetime of the complex. On the other hand, sulfur and nitrogen are relatively soft donor atoms and can form more flexible and weaker bonds with the central cobalt ion. Therefore, complexes **1**−**3** provide new insights into the design and synthesis of Co(II)-SIMs.

The spin-Hamiltonian parameters of each complex determined by dc magnetic susceptibility have shown good agreement among the three methods, especially with regard to the ZFS values (D and E). The relationship between the molecular structure and ZFS was further explored using ab initio CASSCF/NEVPT2, which allowed for a rationalization of the observed ZFS parameters for **1**−**3**. Significant changes are noticed in the experimental spin-Hamiltonian parameters from **1** to **3** with the increase in the size of the halide. Both complexes **1** and **2** display a negative D value of −16.4 cm^{-1} in **1** to −13.8 cm^{-1} in **2**, while complex **3** features a positive D value of +14.6 cm^{-1} as shown in Table 2. The results obtained from computational analysis suggest that the observed changes in the D values are primarily due to distortion in the molecular structure that perturbs the energy levels of Co 3d orbitals and not due to the heavy-atom effect or the halide effect which account for ∼3−4 cm^{-1} variation. The reason for the absence of a noticeable "heavy-atom effect" in the series is attributed to the ionic nature of the Co−X bonds, which limits the halide character in the Co 3d-based MOs.[53] Consequently, the mechanism for enhancing ZFS through cobalt−halide covalency is not applicable for these complexes. The orbitals d_{xy},d_{yz},d_{xz} are essentially nondegenerate for all three complexes, but the gap dramatically widens to ∼2100 cm^{-1} as we go from Cl/Br to I due to the higher degree of structural distortion in the **3** as can be seen from the XRD data. This further contributes to the observation of the geometry of the complex being the key factor in deciding the sign of D. Previous studies have also found that the impact of halide substitution on ZFS is dependent on multiple factors and is not the only factor that determines the trend in the D value of complexes.[32,53−55]

4. CONCLUSIONS

The present study has highlighted the magnetochemistry of three mononuclear Co(II) complexes of general formulas $[Co(L)_2X_2]$ (L= (9*H*-carbazol-9-yl)diphenylphosphine oxide) [X = Cl (**1**), Br (**2**), and I (**3**)] with pseudotetrahedral geometry around the cobalt ion. Combination of magnetic measurements and theoretical studies has unraveled the effect of halide ion substitution on the easy-axis anisotropy and ZFS. Significant uniaxial anisotropy is observed for all the compounds. Under an applied field, slow magnetic relaxation behavior is observed. The ab initio CASSCF/NEVPT2 calculations and magnetostructural correlation studies highlight the importance of structural distortion in controlling the sign and strength of D values in a pseudo tetrahedral geometry. Thus, this study suggests that the magnetic relaxation characteristics may be altered by the central metal ion's local symmetry. It can thus be concluded that the slow magnetic relaxation in these complexes is a result of strong axial and rhombic magnetic anisotropies. Based on the results from this study, one can infer that the halide effect does not always render negative ZFS as presumed earlier. Additionally, this study aids understanding of the distinction between the geometry around the central metal ion and the heavy-atom effect on the magnetic anisotropy of the Co(II) SIMs as well as modifying the magnetic relaxation mechanisms in Co(II) complexes.

5. EXPERIMENTAL SECTION

All reactions were carried out under dry nitrogen using Schlenk techniques with strict exclusion of air and moisture. All solvents were dried and distilled from Na before use. High-purity anhydrous $CoCl_2$ and $CoBr_2$ were purchased from Sigma-Aldrich and used as received, while CoI_2 was prepared using cobalt carbonate and HI and dried in vacuum before use. The ligand used in this study was synthesized using a previously reported procedure.[34] The Fourier transform infrared (FTIR) data were collected on the solid samples using KBr pellets on a PerkinElmer FTIR spectrometer in the 400−4000 cm^{-1} range. The elemental analyses were performed on a Thermoquest Flash EA 1112 series CHNS Elemental Analyzer. Powder X-ray diffraction measurements were recorded on a Philips X'pert Pro (PANalytical) diffractometer. Thermogravimetric analysis was carried out on a PerkinElmer Pyris thermal analysis system under a stream of nitrogen gas at a heating rate of 10 °C min^{-1}. ESI-MS studies were carried out on a Bruker MaXis impact mass spectrometer. UV−visible spectra were obtained on a Shimadzu UV-NIR-3600 spectrophotometer at room temperature. The details of magnetic measurements are described in the SI.

5.1. Synthesis of 1. A toluene solution (30 mL) of anhydrous $CoCl_2$ (0.272 mmol, 35.3 mg) and ligand (9H-carbazol-9-yl)-diphenylphosphine oxide (0.544 mmol, 200 mg) was heated under reflux for 24 h using the Schlenk technique. After cooling down, the reaction mixture was filtered through a ceilite bed under a nitrogen atmosphere. The volume of the reaction was reduced to half under reduced pressure and kept for crystallization at ambient temperature. Blue crystals of **1** were obtained within a week. mp > 250 °C. Yield: 102 mg (43.6%). Elemental analysis calcd (%) for $C_{48}H_{36}Cl_2CoN_2O_2P_2$: C, 66.68; H, 4.20; N, 3.24; observed (%): 66.51; H, 4.56; N, 3.21. FT-IR (as KBr pellets, cm^{-1}): 3053(br),

https://doi.org/10.1021/acs.inorgchem.3c02401
Inorg. Chem. 2023, 62, 18915−18925

2923(s), 1592(s), 1438(vs), 1199(vs), 1127(s), 1109(vs), 993(s), 878(s), 752(vs), 549 (vs).

5.2. Synthesis of 2. Compound **2** was synthesized following the same procedure described above for compound **1** using $CoBr_2$ (0.272 mmol, 60 mg). Dark green crystals of compound **2** were isolated after 2 weeks. mp > 250 °C. Yield: 130 mg (50%). Elemental analysis calcd (%) for $C_{48}H_{36}Br_2CoN_2O_2P_2$: C, 58.25; H, 3.67; N, 2.83; observed (%): 58.63; H, 3.35; N, 2.59. FT-IR (as KBr pellets, cm^{-1}): 3059(br), 2911(w), 1592(m), 1438(s), 1198(s), 1129(vs), 1108(s), 993(s), 725(s), 546(s).

5.3. Synthesis of 3. Compound **3** was synthesized following the same procedure as **1** using CoI_2 (0.272 mmol, 85 mg). Dark green crystals were obtained after a few weeks. mp > 250 °C. Yield: 170 mg (60%). Elemental analysis calcd (%) for $C_{48}H_{36}I_2CoN_2O_2P_2$: C, 55.04; H, 3.46; N, 2.67; observed (%): C, 55.54; H, 3.55; N, 2.35. FT-IR (as KBr pellets, cm^{-1}): 3053(br), 1592(v), 1440(s), 1297(w), 1196(vs), 1124(s), 1105(s), 1028(w), 993(s), 754(s), 548(vs).

5.4. Single-Crystal X-ray Diffraction Studies. X-ray diffraction data were collected on a Rigaku Saturn 724+ CCD diffractometer fitted with microfocus Mo Kα (λ = 0.7107 Å) radiation sources. Rigaku Crystal Clear-SM Expert software was used for data collection. Data integration and indexing were performed with the CrysAlisPro software suite. The OLEX module was used to perform all the calculations.[56] The structures were solved by direct methods using SHELXT 2014/5. The final structure refinement was carried out using full least-squares methods on F^2 using SHELXL-2016/6 software.[57] All nonhydrogen atoms were refined anisotropically. Hydrogen atoms attached to carbon atoms are placed at calculated positions and refined using a riding model. A solvent mask protocol in Olex2 was implemented to account with the remaining electron density corresponding to a disordered molecule of toluene in compound **3**. Crystal data and structure refinement details for **1**−**3** are given in Table S2.

5.5. Computational Details. The X-ray structures served as the basis for all quantum chemistry calculations using ORCA.[58] We employed multireference ab initio computations to determine the nature of low-lying excited states and ZFS parameters. On complexes **1**−**3**, CASSCF calculations with the N-electron valence perturbation (NEVPT2) theory were carried out. The dynamic correlation was recovered by performing NEVPT2 computations on top of the converged CASSCF wave function. A second-order Douglas−Kroll−Hess (DKH) approach was used to tackle the scalar relativistic effects. All these operations were performed using the electron-segmented def2-TZVP basis set for Co, O, Br, and Cl, Sapporo-DKH3-DZP-2012 for I and def2-SVP for the rest of the atoms.[59−61] The calculations were accelerated using the respective auxiliary basis sets and the resolution of identity (RI) approximation. As the D values for **1**−**3** were showing similar trends for model structures and magnetostructural correlation, only CASSCF was performed. Ten quartets and 40 doublets were calculated using the CAS(7,5) active space. Along with computing the SH parameters, we also ran surveys for fitting magnetization data to evaluate the quality of the fit.

■ ASSOCIATED CONTENT

Supporting Information

The Supporting Information is available free of charge at https://pubs.acs.org/doi/10.1021/acs.inorgchem.3c02401.

Additional experimental details, spectral characterization data, X-ray crystallographic details, and additional figures comprising magnetic and computational studies (PDF)

Accession Codes

CCDC 2265710−2265712 contain the supplementary crystallographic data for this paper. These data can be obtained free of charge via www.ccdc.cam.ac.uk/data_request/cif, or by emailing data_request@ccdc.cam.ac.uk, or by contacting The Cambridge Crystallographic Data Centre, 12 Union Road, Cambridge CB2 1EZ, UK; fax: +44 1223 336033.

■ AUTHOR INFORMATION

Corresponding Authors

Gopalan Rajaraman − *Department of Chemistry, Indian Institute of Technology Bombay, Powai 400076 Mumbai, India;* orcid.org/0000-0001-6133-3026; Email: rajaraman@chem.iitb.ac.in

Ramaswamy Murugavel − *Department of Chemistry, Indian Institute of Technology Bombay, Powai 400076 Mumbai, India;* orcid.org/0000-0002-1816-3225; Email: rmv@chem.iitb.ac.in

Authors

Gargi Bhatt − *Department of Chemistry, Indian Institute of Technology Bombay, Powai 400076 Mumbai, India*

Tanu Sharma − *Department of Chemistry, Indian Institute of Technology Bombay, Powai 400076 Mumbai, India*

Sandeep K. Gupta − *University of Göttingen, Institute of Inorganic Chemistry, Göttingen D-37077, Germany;* orcid.org/0000-0003-2432-933X

Franc Meyer − *University of Göttingen, Institute of Inorganic Chemistry, Göttingen D-37077, Germany;* orcid.org/0000-0002-8613-7862

Complete contact information is available at: https://pubs.acs.org/10.1021/acs.inorgchem.3c02401

Notes

The authors declare no competing financial interest.

■ ACKNOWLEDGMENTS

R.M. acknowledges SERB, New Delhi [SPR/2019/001145, CRG/2022/002406, and J. C. Bose Fellowship grant (SB/S2/JCB-85/2014)], for funding the research work. G.R. acknowledges CRG/2022/001697 and SB/SJF/2019-20/12 for funding. G.B. thanks UGC, New Delhi, for a research fellowship and central facilities and SAIF-IIT Bombay for help with various spectral measurements. T.S. is thankful to CSIR for SRF fellowship. S.K.G. thanks the Alexander von Humboldt Foundation and the International Centre of the University of Göttingen for postdoctoral research fellowships. The purchase of the SQUID magnetometer was supported by the DFG (project number 423442764 INST 186/1329-1 FUGG) and the Niedersächsische Ministerium für Wissenschaft und Kultur (MWK).

■ REFERENCES

(1) Sessoli, R.; Gatteschi, D.; Caneschi, A.; Novak, M. A. Magnetic Bistability in a Metal-Ion Cluster. *Nature* **1993**, *365*, 141−143.

(2) Eppley, H. J.; Tsai, H.; de Vries, N.; Folting, K.; Christou, G.; Hendrickson, D. N. High-Spin Molecules: Unusual Magnetic Susceptibility Relaxation Effects in $[Mn_{12}O_{12}(O_2CEt)_{16}(H_2O)_3]$ (S = 9) and the One-Electron Reduction Product (PPh_4)-$[Mn_{12}O_{12}(O_2CEt)_{16}(H_2O)_4]$ (S = 19/2). *J. Am. Chem. Soc.* **1995**, *117*, 301−317.

(3) Boča, R.; Rajnák, C. Unexpected Behavior of Single Ion Magnets. *Coord. Chem. Rev.* **2021**, *430*, 213657.

(4) Meng, Y. S.; Jiang, S. D.; Wang, B. W.; Gao, S. Understanding the Magnetic Anisotropy toward Single-Ion Magnets. *Acc. Chem. Res.* **2016**, *49*, 2381−2389.

(5) Gupta, S. K.; Rajeshkumar, T.; Rajaraman, G.; Murugavel, R. An Air-Stable Dy(III) Single-Ion Magnet with High Anisotropy Barrier and Blocking Temperature. *Chem. Sci.* **2016**, *7* (8), 5181−5191.

(6) Goodwin, C. A. P.; Ortu, F.; Reta, D.; Chilton, N. F.; Mills, D. P. Molecular magnetic hysteresis at 60 kelvin in dysprosocenium. *Nature* **2017**, *548*, 439−442.

(7) Freedman, D. E.; Harman, W. H.; Harris, T. D.; Long, G. J.; Chang, C. J.; Long, J. R. Slow Magnetic Relaxation in a High-Spin Iron(II) Complex. *J. Am. Chem. Soc.* **2010**, *132*, 1224−1225.
(8) Craig, G. A.; Murrie, M. 3D Single-Ion Magnets. *Chem. Soc. Rev.* **2015**, *44*, 2135−2147.
(9) Murrie, M.; Teat, S. J.; Stœckli-Evans, H.; Güdel, H. U. Synthesis and Characterization of a Cobalt(II) Single-Molecule Magnet. *Angew. Chem., Int. Ed.* **2003**, *42*, 4653−4656.
(10) Zadrozny, J. M.; Long, J. R. Slow Magnetic Relaxation at Zero Field in the Tetrahedral Complex $[Co(SPh)_4]^{2-}$. *J. Am. Chem. Soc.* **2011**, *133*, 20732−20734.
(11) Saber, M. R.; Dunbar, K. R. Ligands Effects on the Magnetic Anisotropy of Tetrahedral Cobalt Complexes. *Chem. Commun.* **2014**, *50*, 12266−12269.
(12) Meng, Y. S.; Mo, Z.; Wang, B. W.; Zhang, Y. Q.; Deng, L.; Gao, S. Observation of the Single-Ion Magnet Behavior of d^8 Ions on Two-Coordinate Co(I)-NHC Complexes. *Chem. Sci.* **2015**, *6*, 7156−7162.
(13) Novikov, V. V.; Pavlov, A. A.; Nelyubina, Y. V.; Boulon, M. E.; Varzatskii, O. A.; Voloshin, Y. Z.; Winpenny, R. E. P. A Trigonal Prismatic Mononuclear Cobalt(II) Complex Showing Single-Molecule Magnet Behavior. *J. Am. Chem. Soc.* **2015**, *137*, 9792−9795.
(14) Yao, X. N.; Du, J. Z.; Zhang, Y. Q.; Leng, X. B.; Yang, M. W.; Jiang, S. D.; Wang, Z. X.; Ouyang, Z. W.; Deng, L.; Wang, B. W.; Gao, S. Two-Coordinate Co(II) Imido Complexes as Outstanding Single-Molecule Magnets. *J. Am. Chem. Soc.* **2017**, *139*, 373−380.
(15) Bunting, P. C.; Atanasov, M.; Damgaard-Møller, E.; Perfetti, M.; Crassee, I.; Orlita, M.; Overgaard, J.; Van Slageren, J.; Neese, F.; Long, J. R. A Linear Cobalt(II) Complex with Maximal Orbital Angular Momentum from a Non-Aufbau Ground State. *Science* **2018**, *362*, No. eaat7319.
(16) Vallejo, J.; Viciano-Chumillas, M.; Lloret, F.; Julve, M.; Castro, I.; Krzystek, J.; Ozerov, M.; Armentano, D.; De Munno, G.; Cano, J. Coligand Effects on the Field-Induced Double Slow Magnetic Relaxation in Six-Coordinate Cobalt(II) Single-Ion Magnets (SIMs) with Positive Magnetic Anisotropy. *Inorg. Chem.* **2019**, *58*, 15726−15740.
(17) Kumar, P.; Santalucia, D. J.; Kaniewska-Laskowska, K.; Lindeman, S. V.; Ozarowski, A.; Krzystek, J.; Ozerov, M.; Telser, J.; Berry, J. F.; Fiedler, A. T. Probing the Magnetic Anisotropy of Co(II) Complexes Featuring Redox-Active Ligands. *Inorg. Chem.* **2020**, *59*, 16178−16193.
(18) Gupta, S. K.; Nielsen, H. H.; Thiel, A. M.; Klahn, E. A.; Feng, E.; Cao, H. B.; Hansen, T. C.; Lelièvre-Berna, E.; Gukasov, A.; Kibalin, I.; Dechert, S.; Demeshko, S.; Overgaard, J.; Meyer, F. Multi-Technique Experimental Benchmarking of the Local Magnetic Anisotropy of a Cobalt(II) Single-Ion Magnet. *JACS Au* **2023**, *3*, 429−440.
(19) Murrie, M. Cobalt(II) Single-Molecule Magnets. *Chem. Soc. Rev.* **2010**, *39*, 1986−1995.
(20) Landart-Gereka, A.; Quesada-Moreno, M. M.; Díaz-Ortega, I. F.; Nojiri, H.; Ozerov, M.; Krzystek, J.; Palacios, M. A.; Colacio, E. Large easy-axis magnetic anisotropy in a series of trigonal prismatic mononuclear cobalt (II) complexes with zero-field hidden single-molecule magnet behaviour: the important role of the distortion of the coordination sphere and intermolecular interactions in the slow relaxation. *Inorg. Chem. Front.* **2022**, *9*, 2810−2831.
(21) Landart-Gereka, A.; Quesada-Moreno, M. M.; Palacios, M. A.; Díaz-Ortega, I. F.; Nojiri, H.; Ozerov, M.; Krzystek, J.; Colacio, E. Pushing up the Easy-Axis Magnetic Anisotropy and Relaxation Times in Trigonal Prismatic CoII Mononuclear SMMs by Molecular Structure Design. *Chem. Commun.* **2023**, *59*, 952−955.
(22) Gupta, S. K.; Rao, S. V.; Demeshko, S.; Dechert, S.; Bill, E.; Atanasov, M.; Neese, F.; Meyer, F. Air-Stable Four-Coordinate Cobalt(II) Single-Ion Magnets: Experimental and Ab Initio Ligand Field Analyses of Correlations between Dihedral Angles and Magnetic Anisotropy. *Chem. Sci.* **2023**, *14*, 6355−6374.
(23) Campbell, V. E.; Tonelli, M.; Cimatti, I.; Moussy, J. B.; Tortech, L.; Dappe, Y. J.; Rivière, E.; Guillot, R.; Delprat, S.; Mattana, R.; Seneor, P.; Ohresser, P.; Choueikani, F.; Otero, E.; Koprowiak, F.; Chilkuri, V. G.; Suaud, N.; Guihéry, N.; Galtayries, A.; Miserque, F.; Arrio, M. A.; Sainctavit, P.; Mallah, T. Engineering the Magnetic Coupling and Anisotropy at the Molecule-Magnetic Surface Interface in Molecular Spintronic Devices. *Nat. Commun.* **2016**, *7*, 13646.
(24) Coronado, E. Molecular Magnetism: From Chemical Design to Spin Control in Molecules, Materials and Devices. *Nat. Rev. Mater.* **2019**, *5* (2), 87−104.
(25) Sarkar, A.; Dey, S.; Rajaraman, G. Role of Coordination Number and Geometry in Controlling the Magnetic Anisotropy in FeII, CoII, and NiII Single-Ion Magnets. *Chem.—Eur. J.* **2020**, *26*, 14036−14058.
(26) Karunadasa, H. I.; Arquero, K. D.; Berben, L. A.; Long, J. R. Enhancing the Magnetic Anisotropy of Cyano-Ligated Chromium(II) and Chromium(III) Complexes via Heavy Halide Ligand Effects. *Inorg. Chem.* **2010**, *49*, 4738−4740.
(27) Boča, R.; Miklovič, J.; Titiš, J. Simple Mononuclear Cobalt(II) Complex: A Single-Molecule Magnet Showing Two Slow Relaxation Processes. *Inorg. Chem.* **2014**, *53*, 2367−2369.
(28) Vaidya, S.; Shukla, P.; Tripathi, S.; Rivière, E.; Mallah, T.; Rajaraman, G.; Shanmugam, M. Substituted versus Naked Thiourea Ligand Containing Pseudotetrahedral Cobalt(II) Complexes: A Comparative Study on Its Magnetization Relaxation Dynamics Phenomenon. *Inorg. Chem.* **2018**, *57*, 3371−3386.
(29) Tripathi, S.; Vaidya, S.; Ansari, K. U.; Ahmed, N.; Rivière, E.; Spillecke, L.; Koo, C.; Klingeler, R.; Mallah, T.; Rajaraman, G.; Shanmugam, M. Influence of a Counteranion on the Zero-Field Splitting of Tetrahedral Cobalt(II) Thiourea Complexes. *Inorg. Chem.* **2019**, *58*, 9085−9100.
(30) Ye, S.; Neese, F. How Do Heavier Halide Ligands Affect the Signs and Magnitudes of the Zero-Field Splittings in Halogenonickel-(II) Scorpionate Complexes? A Theoretical Investigation Coupled to Ligand-Field Analysis. *J. Chem. Theory Comput.* **2012**, *8*, 2344−2351.
(31) Smolko, L.; Černák, J.; Dušek, M.; Titiš, J.; Boča, R. Tetracoordinate Co(II) Complexes Containing Bathocuproine and Single Molecule Magnetism. *New J. Chem.* **2016**, *40*, 6593−6598.
(32) Devkota, L.; Santalucia, D. J.; Wheaton, A. M.; Pienkos, A. J.; Lindeman, S. V.; Krzystek, J.; Ozerov, M.; Berry, J. F.; Telser, J.; Fiedler, A. T. Spectroscopic and Magnetic Studies of Co(II) Scorpionate Complexes: Is There a Halide Effect on Magnetic Anisotropy? *Inorg. Chem.* **2023**, *62*, 5984−6002.
(33) Kumar Sahu, P.; Kharel, R.; Shome, S.; Goswami, S.; Konar, S. Understanding the Unceasing Evolution of Co(II) Based Single-Ion Magnets. *Coord. Chem. Rev.* **2023**, *475*, 214871.
(34) Tao, Y.; Xiao, J.; Zheng, C.; Zhang, Z.; Yan, M.; Chen, R.; Zhou, X.; Li, H.; An, Z.; Wang, Z.; Xu, H.; Huang, W. Dynamically Adaptive Characteristics of Resonance Variation for Selectively Enhancing Electrical Performance of Organic Semiconductors. *Angew. Chem., Int. Ed.* **2013**, *52* (40), 10491−10495.
(35) Mondal, A. K.; Sundararajan, M.; Konar, S. A New Series of Tetrahedral Co(II) Complexes $[CoLX_2]$ (X = NCS, Cl, Br, I) Manifesting Single-Ion Magnet Features. *Dalton Trans.* **2018**, *47*, 3745−3754.
(36) Mitsuhashi, R.; Hosoya, S.; Sunatsuki, Y.; Suzuki, T.; Mikuriya, M. Field-Induced Single-Ion Magnet Behaviors in 1-Dimensionally Assembled Tetrahedral Cobalt(II) Complexes with Halide Donors. *Inorg. Chim. Acta* **2022**, *529*, 120667.
(37) Mantanona, A. J.; Tolentino, D. R.; Cay, K. S.; Gembicky, M.; Jazzar, R.; Bertrand, G.; Rinehart, J. D. Tuning Electronic Structure through Halide Modulation of Mesoionic Carbene Cobalt Complexes. *Dalton Trans.* **2020**, *49*, 2426−2430.
(38) Titiš, J.; Miklovič, J.; Boča, R. Magnetostructural Study of Tetracoordinate Cobalt(II) Complexes. *Inorg. Chem. Commun.* **2013**, *35*, 72−75.
(39) Krzystek, J.; Zvyagin, S. A.; Ozarowski, A.; Fiedler, A. T.; Brunold, T. C.; Telser, J. Definitive Spectroscopic Determination of Zero-Field Splitting in High-Spin Cobalt(II). *J. Am. Chem. Soc.* **2004**, *126*, 2148−2155.
(40) Yang, F.; Zhou, Q.; Zhang, Y.; Zeng, G.; Li, G.; Shi, Z.; Wang, B.; Feng, S. Inspiration from Old Molecules: Field-Induced Slow

Magnetic Relaxation in Three Air-Stable Tetrahedral Cobalt(II) Compounds. *Chem. Commun.* **2013**, *49*, 5289−5291.
(41) Smolko, L.; Černák, J.; Dušek, M.; Miklovič, J.; Titiš, J.; Boča, R. Three Tetracoordinate Co(II) Complexes $[Co(Biq)X_2]$ (X = Cl, Br, I) with Easy-Plane Magnetic Anisotropy as Field-Induced Single-Molecule Magnets. *Dalton Trans.* **2015**, *44*, 17565−17571.
(42) Nicholls, D. *Complexes and First-Row Transition Elements*; Macmillan Education UK, 1974.
(43) Llunell, M.; Casanova, D.; Cirera, J.; Bofill, J. M.; Alemany, P.; Alvarez, S. *SHAPE*. version 2.1: Barcelona, 2013.
(44) Bill, E. *julX_2s, Simulation of Molecular Magnetic Data Software*; Max-Planck Institute for Bioinorganic Chemistry: Mülheim, Ruhr, 2014.
(45) Reta, D.; Chilton, N. F. Uncertainty Estimates for Magnetic Relaxation Times and Magnetic Relaxation Parameters. *Phys. Chem. Chem. Phys.* **2019**, *21*, 23567−23575.
(46) Vaidya, S.; Singh, S. K.; Shukla, P.; Ansari, K.; Rajaraman, G.; Shanmugam, M. Role of Halide Ions in the Nature of the Magnetic Anisotropy in Tetrahedral CoII Complexes. *Chem.—Eur. J.* **2017**, *23*, 9546−9559.
(47) Ruamps, R.; Batchelor, L. J.; Maurice, R.; Gogoi, N.; Jiménez-Lozano, P.; Guihéry, N.; de Graaf, C.; Barra, A. L.; Sutter, J. P.; Mallah, T. Origin of the Magnetic Anisotropy in Heptacoordinate NiII and CoII Complexes. *Chem.—Eur. J.* **2013**, *19*, 950−956.
(48) Gomez-Coca, S.; Cremades, E.; Aliaga-Alcalde, N.; Ruiz, E. Mononuclear Single-Molecule Magnets: Tailoring the Magnetic Anisotropy of First-Row Transition-Metal Complexes. *J. Am. Chem. Soc.* **2013**, *135*, 7010−7018.
(49) Ruamps, R.; Batchelor, L. J.; Guillot, R.; Zakhia, G.; Barra, A. L.; Wernsdorfer, W.; Guihéry, N.; Mallah, T. Ising-Type Magnetic Anisotropy and Single Molecule Magnet Behaviour in Mononuclear Trigonal Bipyramidal Co(II) Complexes. *Chem. Sci.* **2014**, *5*, 3418−3424.
(50) Vaidya, S.; Upadhyay, A.; Singh, S. K.; Gupta, T.; Tewary, S.; Langley, S. K.; Walsh, J. P. S.; Murray, K. S.; Rajaraman, G.; Shanmugam, M. A Synthetic Strategy for Switching the Single Ion Anisotropy in Tetrahedral Co(II) Complexes. *Chem. Commun.* **2015**, *51*, 3739−3742.
(51) Korchagin, D. V.; Shilov, G. V.; Aldoshin, S. M.; Morgunov, R. B.; Talantsev, A. D.; Yureva, E. A. Halogen Atom Effect on the Magnetic Anisotropy of Pseudotetrahedral Co(II) Complexes with a Quinoline Ligand. *Polyhedron* **2015**, *102*, 147−151.
(52) Suturina, E. A.; Nehrkorn, J.; Zadrozny, J. M.; Liu, J.; Atanasov, M.; Weyhermüller, T.; Maganas, D.; Hill, S.; Schnegg, A.; Bill, E.; Long, J. R.; Neese, F. Magneto-Structural Correlations in Pseudotetrahedral Forms of the $[Co(SPh)_4]^{2-}$ Complex Probed by Magnetometry, MCD Spectroscopy, Advanced EPR Techniques, and Ab Initio Electronic Structure Calculations. *Inorg. Chem.* **2017**, *56*, 3102−3118.
(53) Coste, S. C.; Vlaisavljevich, B.; Freedman, D. E. Magnetic Anisotropy from Main-Group Elements: Halides versus Group 14 Elements. *Inorg. Chem.* **2017**, *56* (14), 8195−8202.
(54) Duboc, C.; Phoeung, T.; Zein, S.; Pécaut, J.; Collomb, M. N.; Neese, F. Origin of the Zero-Field Splitting in Mononuclear Octahedral Dihalide MnII Complexes: An Investigation by Multifrequency High-Field Electron Paramagnetic Resonance and Density Functional Theory. *Inorg. Chem.* **2007**, *46*, 4905−4916.
(55) Weller, R.; Atanasov, M.; Demeshko, S.; Chen, T. Y.; Mohelsky, I.; Bill, E.; Orlita, M.; Meyer, F.; Neese, F.; Werncke, C. G. On the Single-Molecule Magnetic Behavior of Linear Iron(I) Arylsilylamides. *Inorg. Chem.* **2023**, *62*, 3153−3161.
(56) Dolomanov, O. V.; Bourhis, L. J.; Gildea, R. J.; Howard, J. A. K.; Puschmann, H. *OLEX2*: a complete structure solution, refinement and analysis program. *J. Appl. Crystallogr.* **2009**, *42* (2), 339−341.
(57) Sheldrick, G. M. Crystal Structure Refinement with SHELXL. *Acta Crystallogr., Sect. C: Struct. Chem.* **2015**, *71*, 3−8.
(58) Neese, F. The ORCA Program System. *Wiley Interdiscip. Rev.: Comput. Mol. Sci.* **2012**, *2*, 73−78.
(59) Weigend, F.; Ahlrichs, R. Balanced Basis Sets of Split Valence, Triple Zeta Valence and Quadruple Zeta Valence Quality for H to Rn: Design and Assessment of Accuracy. *Phys. Chem. Chem. Phys.* **2005**, *7*, 3297−3305.
(60) Weigend, F. Accurate Coulomb-Fitting Basis Sets for H to Rn. *Phys. Chem. Chem. Phys.* **2006**, *8*, 1057−1065.
(61) Hellweg, A.; Hättig, C.; Höfener, S.; Klopper, W. Optimized Accurate Auxiliary Basis Sets for RI-MP2 and RI-CC2 Calculations for the Atoms Rb to Rn. *Theor. Chem. Acc.* **2007**, *117*, 587−597.

https://doi.org/10.1021/acs.inorgchem.3c02401
Inorg. Chem. 2023, 62, 18915−18925